Fabrication and Characterization of Antimony doped Iron oxide Nanoparticles

Tahir Jamal[1], Syed Farhan Hasany[2], Muhammad Amir[3,*], Maryam Tahir[1], Sabahat Javed[1], Ume Sehar[1],

[1] Department of Physics, NEDUET, Karachi, Pakistan
[2] Department of Chemistry, NEDUET, Karachi, Pakistan
[3] Department of Textile Engineering, NEDUET, Karachi, Pakistan
[*]Corresponding author: qureshi@neduet.edu.pk

Abstract

Antimony oxide (Sb_2O_3) and Antimony-doped iron oxide ($Sb - Fe_2O_3$) nanomaterials of different (2 & 3 %) concentrations were fabricated by wet synthesis technique and characterized by FTIR, X-RD and X-RF techniques. X-RD results showed uniform Iron oxide nanocrystals of almost 15 nm, whereas FTIR and X-RF were employed to detect the elemental composition of Antimony in doped ($Sb - Fe_2O_3$) samples.

Keywords—X-RD; FTIR; X-RF; antimony oxide; antimony-doped iron oxide; nanoparticles

1 Introduction

Nanotechnology has empowered researchers to produce new materials at nanoscale with enhanced properties by manipulating and controlling shapes and sizes. Many techniques have been employed for the synthesis of size-controlled nanomaterials and respective characterizations [1-9].

The fabrication of discrete iron oxide nanomaterials with a size range of 2-20 nm is of great significance in number of applications. An iron oxide nanomaterial with partly distorted structures in comparison to its defect-free polymorph undergoes cat-ion attachment reactions with no larger variation in the crystal structure. Modifying the physicochemical behavior of nanomaterials by transition metals doping [10, 11], including antimony could be beneficial for multiple applications. Additionally, antimony doping could bring good control in the material usage for future electro-conductive applications, which will ultimately result in superior control of toxicity and prospective applications [12]. The present study aims to investigate the doping mechanism of antimony in the crystal lattice of Iron oxide nanomaterial because of its potential application in electro-conductive studies. A single pot scheme shows precipitation followed by annealing at low temperatures for a shorter period of time to achieve fully grown and smaller Nanocrystals.

ISSN: 2523-0379 (Online), ISSN: 1605-8607 (Print)
DOI: https://doi.org/10.52584/QRJ.2101.08

2 Experimental

2.1 Materials

Analytical-grade chemicals and reagents were utilized in this investigation exactly as they were received. Surface activation of a predetermined quantity of ferric nitrate ($Fe(NO_3)_3.9H_2O$) was done for one hour under a controlled environment. A molar mixture of ($Fe(NO_3)_3.9H_2O$) and Antimony oxide (Sb_2O_3), was added to (25 mL) nitrogen bubbled ultrapure water and stirred for 20 minutes. Dropwise additions of ammonium hydroxide (NH4OH) were made to the solution in a controlled environment at room temperature until the pH reached 9 to 9.5. The aforementioned sol was centrifuged at 7000 rpm for 10 minutes to create a colloidal solution after being aged for 10 minutes. To eliminate surplus water from the sample, the sediment was dried using a water bath at 90 °C for 30 minutes. The dried sample was calcined in the air at 500 °C for 15 minutes to get the desired doped material.

2.2 Characterizations

Nano metric product was characterized after production. The X-ray diffraction (X-RD) pattern of the produced Hematite nanoparticles was recorded for structural size and shape. Additionally, the doped

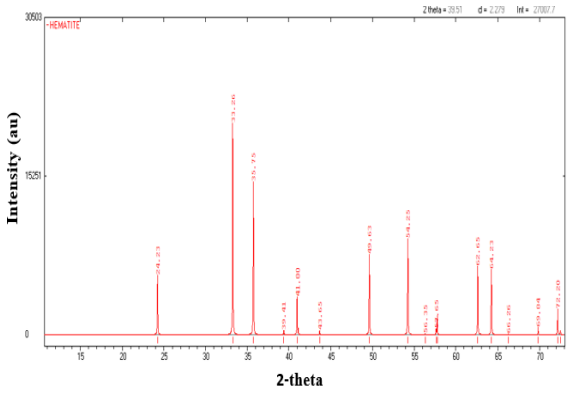

Fig. 1: X-ray diffractogram of Hematite Nanoparticles

nanomaterial was further studied by X-RF and FTIR to ascertain the composition of the prepared material. Furthermore, a vibrating sample magnetometer (VSM) was used to study the magnetic properties of synthesized nanomaterial.

3 Results and Discussions

X-RD analysis:

By using X-RD, the crystallinity, phase and composition of the synthesized hematite nanomaterial was determined. Cu-K X'PERT Pro Diffractometer was employed for this, and the sample was analyzed in the range of 10 to 80 diffraction angles (2-theta). Scherer's equation was applied to determine the crystal size. X-RD results are shown in figure 1. The two characteristic peaks at 33 and 35, 2-theta confirm the formation of Hematite Nanoparticles. The average crystal size calculated by substituting all the related values in Scherer's equation was found to be 15 nm [13, 14].

FTIR analysis:

FTIR spectroscopy $(4000 - 500cm_{-1})$ was performed to examine the bonding in the synthesized hematite and doped ferrite nanoparticles respectively. The absorbance intensity was plotted against wavelength as shown in Figures 2 (a-c).

The data demonstrate a wider range of bonds $(3400 - 1620cm_{-1})$, which suggests the presence of O-H bond connected to the surface of cobalt oxide. This indicates that throughout the manufacturing process, hematite nanoparticles absorbed water molecules but the majority of the water was removed during calcination. The peaks in the spectra are not broad, which may be related to the fact that there are less water molecules present in the crystal[13]. FTIR spectra clarify metal ions occupancy at both tetrahedral and octahedral sites with respect to

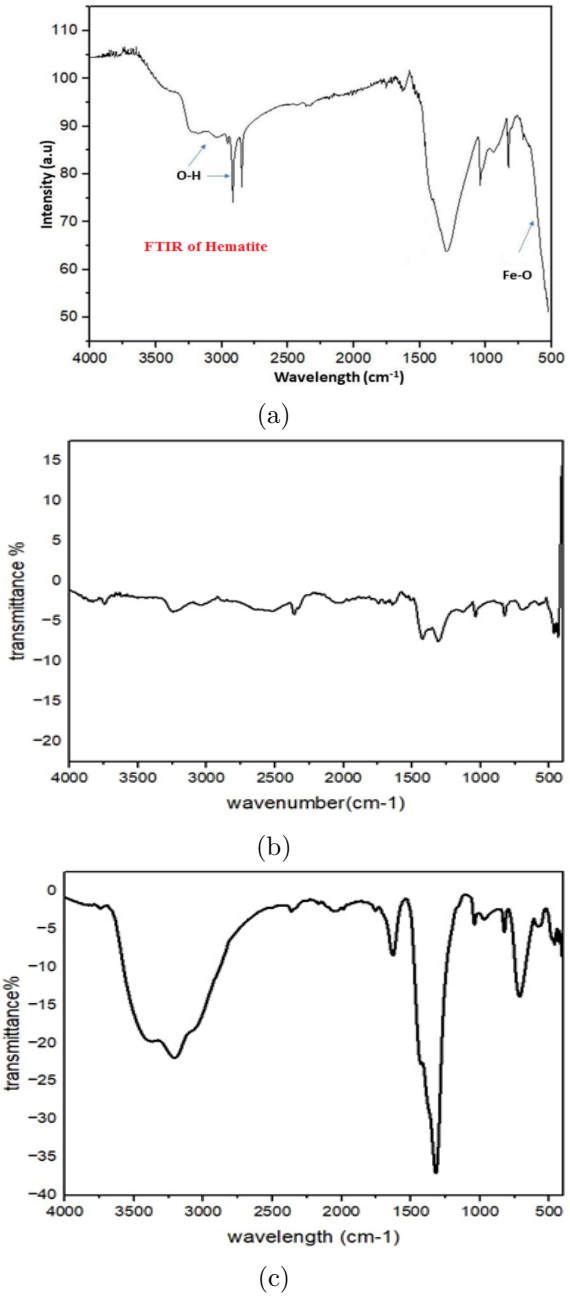

Fig. 2: (a) FTIR spectra of Hematite Nanoparticles, (b) Graphical result of 2% antimony doped Iron Oxide Nanomaterial and (c) Graphical result of 3% antimony doped Iron Oxide Nanomaterial

the geometrical configuration of nearest oxygen in the lattice. Therefore, the nanoparticles have spinel structure.

Figure 2 (b&c) show the FTIR results of antimony doped hematite particles. The stretching vibrations of Sb-O functional groups infrared are observed in ranges from $(500to800cm_{-1})$ and 900 to 1250 cm-1, respectively.

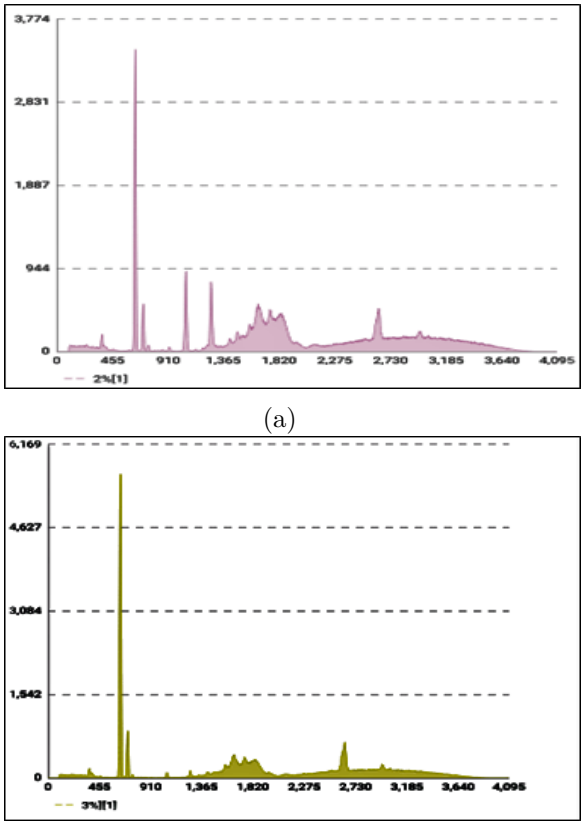

Fig. 3: (a) The X-RF spectra for 2% Sb doped Fe_2O_3, and (b) The X-RF spectra for 3% Sb doped Fe_2O_3

X-RF analysis:

The samples were analyzed by the energy dispersive X-RF at $45V$ and current ranges from $40\mu amp$ to 120 μamp. The concentration of hematite and antimony were quantized by characteristic peaks at $2730KeV(K\alpha)$ and at $400KeV(L\alpha)$, in a 'Mineral' mode through a standard less, fundamental parameters-based $\alpha - coefficient$ correction model. Figures 3 (a & b), Table 1 and Table 2 show X-RF for 2% and 3% doped hematite where the elemental composition of Iron and Sb are very similar to the molar ratios being employed during fabrication.

4 Conclusion

Hematite and antimony doped hematite nanomaterials were fabricated successfully by wet chemical technique. Smaller particle size (15 nm) as calculated by X-RD made it suitable for various semiconducting and sensing applications. Surface water molecules and the distinct interaction between Antimony, Iron and Oxygen in the crystal lattice were confirmed by FTIR. X-RF technique found elemental composition ratios very near to the molar ratios being employed for synthesis. The product has potential application in storage devices, for which additional study is required.

TABLE 1: X-RF spectrum data for (2%) Sb doped Fe_2O_3

Element	Content	Detection limit	Error
Mg(%)	0.77	0.00	0.05
Al(%)	0.47	0.00	0.02
Si(%)	3.27	0.00	0.02
P(%)	0.10	0.00	0.00
S(%)	1.09	0.00	0.01
K(%)	0.08	0.00	0.00
Ca(%)	0.00	0.00	0.00
Ti(%)	0.08	0.00	0.00
V(%)	0.00	0.00	0.00
Cr(%)	0.00	0.00	0.00
Mn(%)	0.00	0.00	0.00
Fe(%)	4.18	0.00	0.06
Co(%)	0.00	0.00	0.00
Ni(%)	0.00	0.00	0.00
Cu(%)	0.00	0.00	0.00
Zn(%)	0.01	0.00	0.00
As(%)	0.00	0.00	0.00
Se(%)	0.00	0.00	0.00
Sn(%)	0.00	0.00	0.00
Sb(%)	0.15	0.00	0.00
Ag(%)	0.01	0.00	0.00
Mo(%)	0.00	0.00	0.00
Zr(%)	0.01	0.00	0.00
Rb(%)	0.00	0.00	0.00
Sr(%)	0.01	0.00	0.00
Ba(%)	0.08	0.00	0.00
W(%)	0.08	0.00	0.01
Ta(%)	0.00	0.00	0.00
Au(PPM)	0.00	0.00	0.00
Hg(PPM)	0.00	0.00	0.00
Pb(%)	0.28	0.00	0.00
Cd(%)	0.00	0.00	0.00

References

[1] D. D. Awschalom and D. P. DiVincenzo, "Complex dynamics of mesoscopic magnets," Physics Today, vol. 48, no. 4, pp. 43-48, 1995.

[2] K. Raj and R. Moskowitz, "Commercial applications of ferrofluids," Journal of Magnetism Magnetic Materials, vol. 85, no. 1-3, pp. 233-245, 1990.

[3] I. M. Billas, A. Chatelain, and W. A. de Heer, "Magnetism from the atom to the bulk in iron, cobalt, and nickel clusters," Science, vol. 265, no. 5179, pp. 1682-1684, 1994.

TABLE 2: X-RF spectrum data for (3%) Sb doped Fe_2O_3

Element	Content	Detection limit	Error
Mg(%)	1.26	0.00	0.09
Al(%)	0.00	0.00	0.00
Si(%)	2.90	0.00	0.02
P(%)	0.09	0.00	0.00
S(%)	0.00	0.00	0.00
K(%)	0.08	0.00	0.00
Ca(%)	0.00	0.00	0.00
Ti(%)	0.09	0.00	0.00
V(%)	0.00	0.00	0.00
Cr(%)	0.00	0.00	0.00
Mn(%)	0.00	0.00	0.00
Fe(%)	6.66	0.00	0.10
Co(%)	0.00	0.00	0.00
Ni(%)	0.00	0.00	0.00
Cu(%)	0.00	0.00	0.00
Zn(%)	0.00	0.00	0.00
As(%)	0.00	0.00	0.00
Se(%)	0.00	0.00	0.00
Sn(%)	0.00	0.00	0.00
Sb(%)	0.22	0.00	0.00
Ag(%)	0.01	0.00	0.00
Mo(%)	0.00	0.00	0.00
Zr(%)	0.00	0.00	0.00
Rb(%)	0.00	0.00	0.00
Sr(%)	0.01	0.00	0.00
Ba(%)	0.08	0.00	0.00
W(%)	0.09	0.00	0.01
Ta(%)	0.00	0.00	0.00
Au(PPM)	0.00	0.00	0.00
Hg(PPM)	0.00	0.00	0.00
Pb(%)	0.02	0.00	0.00
Cd(%)	0.00	0.00	0.00

[4] L. Berger, G. Bergmann, and R. O'Handley, "Modern Magnetic Materials Principles and Applications," ed: Wiley-Interscience, New York Wiley, New York, 1999.

[5] S. F Hasany, N. H Abdurahman, and A. R Sunarti, "Wet Chemical Approach for Vanadium Doped Maghemite (Fe2-xVxO3) Nanocrystals," Current Nanoscience, vol. 12, no. 5, pp. 617-620, 2016.

[6] R. Hergt, R. Hiergeist, I. Hilger, and W. Kaiser, "Magnetic nanoparticles for thermoablation," Recent Res. Dev. Mater. Sci, vol. 3, pp. 723-742, 2002.

[7] R. Dronskowski, "The little maghemite story: A classic functional material," Advanced Functional Materials, vol. 11, no. 1, pp. 27-29, 2001.

[8] A. K. Gupta and M. Gupta, "Synthesis and surface engineering of iron oxide nanoparticles for biomedical applications," Biomaterials, vol. 26, no. 18, pp. 3995-4021, 2005.

[9] M. Abdullah, S. Hasany, M. Amir Qureshi, and S. Hussain, "Cost-Effective Synthesis of Cobalt Ferrite Nanoparticles by Sol-Gel Technique," in Materials Science Forum, 2022, vol. 1067, pp. 213-219: Trans Tech Publ.

[10] E. V. Groman, J. C. Bouchard, C. P. Reinhardt, and D. E. Vaccaro, "Ultrasmall mixed ferrite colloids as multidimensional magnetic resonance imaging, cell labeling, and cell sorting agents," Bioconjugate chemistry, vol. 18, no. 6, pp. 1763-1771, 2007.

[11] B. P. Hahn, J. W. Long, and D. R. Rolison, "Something from nothing: enhancing electrochemical charge storage with cation vacancies," Accounts of chemical research, vol. 46, no. 5, pp. 1181-1191, 2013.

[12] R. T. Shannon and C. T. Prewitt, "Effective ionic radii in oxides and fluorides," Acta Crystallographica Section B: Structural Crystallography Crystal Chemistry, vol. 25, no. 5, pp. 925-946, 1969.

[13] G. Huang, C.-H. Lu, and H.-H. Yang, "Magnetic nanomaterials for magnetic bioanalysis," in Novel nanomaterials for biomedical, environmental and energy applications: Elsevier, 2019, pp. 89-109.

[14] S. F. Hasany, N. Abdurahman, A. Sunarti, and A. Kumar, "Non-covalent assembly of maghemite-multiwalled carbon nanotubes for efficient lead removal from aqueous solution," Australian Journal of Chemistry, vol. 66, no. 11, pp. 1440-1446, 2013.